

STAR FORMATION IN SHOCK-COMPRESSED LAYERS

BRUCE G. ELMEGREEN* AND DEBRA MELOY ELMEGREEN†

Center for Astrophysics, Harvard College Observatory and Smithsonian Astrophysical Observatory

Received 1977 July 5; accepted 1977 September 12

ABSTRACT

Details of the gravitational collapse of compressed gas behind an isothermal shock are presented. The growth rate of an unstable mode is given as a function of its wavelength for a single-parameter family of layers. Simple formulae for the maximum growth rates, for the wavelength at which this maximum occurs, and for the critically unstable wavelength are given as functions of the model parameter.

The astrophysical implications of these results are discussed. The minimum unstable mass in the plane-parallel case was found to be stable, if it collapses to a pressure-bounded isothermal sphere. The mass of the most rapidly growing instability is also stable as a sphere, unless the column density in this layer σ is sufficiently large in proportion to the square root of the external pressure. A criterion is derived for this dominant, plane-parallel instability to lead to an unstable sphere. It is possible that this criterion marks the beginning of rapid star formation behind a shock. The maximum mass of a fragment that can collapse in a specified time τ is also determined. This maximum mass is independent of the sound velocity in the layer and of the external pressure. It depends sensitively on both τ and σ . Although magnetic fields are not included in the calculation, their influence on the results is briefly discussed.

Subject headings: shock waves — stars: formation

I. INTRODUCTION

The suggestion that stars may form as a result of gravitational instabilities behind shocks is currently receiving some observational support. Large-scale shocks associated with spiral density waves have long been cited as precursors of star formation in spiral arms (e.g., Roberts 1969; Woodward 1976), but it is now becoming evident that shock-induced star formation may also occur regularly on a much smaller scale. In the distribution of stars and molecular clouds associated with M17 (Lada *et al.* 1976; Lada 1976; Elmegreen and Lada 1977), W3 (Elmegreen and Lada 1977), M42 (Orion) (Elmegreen and Lada 1977; Kutner *et al.* 1977), and NGC 281 (Elmegreen and Lada 1978), and in small regions of NGC 7538 (Habing, Israel, and de Jong 1972), the conspicuous position of star-forming regions adjacent to ionization fronts suggests that shocks from slowly expanding H II regions can trigger star formation. In NGC 1333 (Loren 1976), shocks in the region between two colliding clouds may have induced star formation. Around the Gum Nebula (Schwartz 1977) and in CMa R1 (Herbst and Assousa 1977), the presence of newly formed stars in regions adjacent to suspected supernova remnants is suggestive that a supernova shock has triggered the star-forming event in a nearby cloud.

The implications of such forced mechanisms of star formation are overwhelming. In the first place, chain reactions of star-forming events are possible (Ögelman and Maran 1976; Elmegreen and Lada 1977), leading to recognizable patterns in star clusters (e.g., the subgroups in the Orion OB association [see Blaauw 1964]) or perhaps spiral structure in galaxies (Mueller and Arnett 1976). Many detailed properties related to the ages and relative positions of OB subgroups and star-forming regions were shown by Elmegreen and Lada (1977) to be a result of shocks that propagate along a primordial cloud's magnetic field.

Equally important is the implication that many different dynamical processes may be involved in cloud and star formation. In that case, large-scale spatial distributions of star-forming activity, as shown, for example, by chemical composition gradients in the Galaxy (Jensen, Strom, and Strom 1976), may be related to the spatial distribution of a *variety* of interstellar processes. Not only should we consider star-forming shocks that may be a result of spiral density waves, but also we should study the galactic distribution of supernova events or of large-scale variations in the sizes or pressures of H II regions.

Obviously, a thorough investigation of star formation in shocked regions is warranted. The purpose of this paper is to determine the growth rates and masses of perturbations in compressed, isothermal, plane-parallel layers with no magnetic fields. This is done by numerically calculating the dispersion relation for gravitational instabilities in a pressure-bounded layer. The results will be compared in one limiting case with the work of Simon

* Junior Fellow, Harvard Society of Fellows.

† Amelia Earhart Fellow, Zonta International.

(1965*a*), who derived the dispersion relation for an unbounded, plane-parallel layer. Comparison to an approximate solution in another limiting case, when the layer is not significantly self-gravitating, provides a second check. Simple expressions for the maximum growth rates and for the wavelength of the mode at which this maximum growth occurs are given as functions of layer size and external pressure.

The results are applied to estimate the behavior of the compressed layers that occur behind isothermal shocks in astrophysical situations. The conditions for gravitational instabilities and star formation behind shocks that are derived here are a refinement of those given by Elmegreen and Lada (1977).

The equations of hydrostatic equilibrium, the perturbation equations, and the boundary conditions used here are the same as those given by other authors (e.g., Goldreich and Lynden-Bell 1965, hereafter GLB; Simon 1965*a*). The details of these equations are presented in § II. A discussion of the numerical methods used to solve them is deferred to Appendix A. The primary results of this work are shown in the figures of § III, and the limits of application to shocks are discussed in § IV. Several conclusions pertaining to gravitational collapse and star formation in shocked gas are then given in § V. The possible role of magnetic fields is discussed in § VI. These results are summarized in § VII.

II. CALCULATIONS

The hydrostatic equilibrium and marginal stability of infinitely extended plane-parallel layers have been understood since the work of Spitzer (1942) and Ledoux (1951). GLB gave the perturbation equations and boundary conditions for a pressure-bounded, self-gravitating gas layer that rotates around an axis. Simon has given similar equations with and without rotation (Simon 1965*a, b*). In this section, we follow the derivations of these authors.

a) Hydrostatic Equilibrium

In terms of the potential ψ , mass density ρ , pressure P , and constant sound velocity c , the equations of hydrostatic equilibrium may be written

$$\nabla\psi_0 - \frac{1}{\rho_0} \nabla P_0 = 0, \quad (1)$$

$$\nabla^2\psi_0 = -4\pi G\rho_0, \quad (2)$$

$$P = c^2\rho, \quad (3)$$

where the subscripts 0 refer to nonperturbed quantities. The distributions of ψ_0 , ρ_0 , or P_0 inside the layer are completely specified by these three equations and by the external pressure P_{ext} and the total mass column density of the plane, σ .

It is convenient to transform the physical variable z , measured perpendicular to the plane, to a dimensionless variable μ given by

$$\mu = \tanh(z/H), \quad (4)$$

where H is the scale height determined by the density ρ_{00} at the point $z = \mu = 0$:

$$H = c(2\pi G\rho_{00})^{-1/2}. \quad (5)$$

The general solution to equations (1)–(3) may then be written

$$\rho(\mu) = \rho_{00}(1 - \mu^2), \quad (6)$$

where μ varies between the limits $\pm A$ (< 1), which are determined by the external pressure and the central density:

$$A = \left(1 - \frac{P_{\text{ext}}}{\rho_{00}c^2}\right)^{1/2}. \quad (7)$$

The total mass column density in the layer is determined by the integral of ρ over z and becomes

$$\sigma = 2\rho_{00}HA. \quad (8)$$

The central density is thus

$$\rho_{00} = (P + \frac{1}{2}\pi G\sigma^2)/c^2. \quad (9)$$

b) Perturbations around Hydrostatic Equilibrium

Perturbations around equations (1)–(3) require the inclusion of time-dependent terms and of the continuity equation. We let the subscript 1 on variables ψ , ρ , and P denote small perturbations of the potential, density, and

pressure; and \mathbf{u}' will denote a small perturbed velocity. The perturbed equation of motion for the isothermal case then becomes, to first order in the perturbation (GLB),

$$\frac{\partial \mathbf{u}'}{\partial t} = \nabla \left(\hat{\psi}_1 - c^2 \frac{\hat{\rho}_1}{\rho_0} \right). \quad (10)$$

The equation of continuity and Poisson's equation are similarly

$$\frac{\partial \hat{\rho}_1}{\partial t} + \nabla \cdot (\rho_0 \mathbf{u}') = 0, \quad (11)$$

$$\nabla^2 \hat{\psi}_1 = -4\pi G \hat{\rho}_1. \quad (12)$$

The perturbation is now assumed to be of the form

$$\hat{\psi}_1(x, z, t) = \psi_1(z) \exp(i\omega t + ikx) \quad (13)$$

for variable x measured parallel to the layer. Hereafter, variables without a caret or a prime have only a z (or μ) dependence. In terms of the variable z , equations (10)–(12) become

$$i\omega u_x = ik \left(\psi_1 - c^2 \frac{\rho_1}{\rho_0} \right), \quad (14)$$

$$i\omega u_z = \frac{d}{dz} \left(\psi_1 - c^2 \frac{\rho_1}{\rho_0} \right), \quad (15)$$

$$i\omega \rho_1 + ik\rho_0 u_x + \frac{d}{dz} (\rho_0 u_z) = 0, \quad (16)$$

$$\frac{d^2}{dz^2} \psi_1 - k^2 \psi_1 = -4\pi G \rho_1. \quad (17)$$

The units of potential are taken to be c^2 , while H , c , and $(4\pi G \rho_{00})^{-1/2} = 2^{-1/2} H/c$ are the units of distance, velocity, and time, respectively. Then with

$$\Omega = \omega(4\pi G \rho_{00})^{-1/2}, \quad (18)$$

$$\nu = kH, \quad (19)$$

and using the transformation

$$\frac{d}{dz} = \frac{1}{H} (1 - \mu^2) \frac{d}{d\mu}, \quad (20)$$

we obtain from equations (14)–(17) a single equation for the normalized perturbed potential $\psi(\mu)$:

$$(1 - \mu^2)^4 \frac{d^4}{d\mu^4} \psi - 10\mu(1 - \mu^2)^3 \frac{d^3}{d\mu^3} \psi + (20\mu^2 - 4 + 2\Omega^2 - 2\nu^2)(1 - \mu^2)^2 \frac{d^2}{d\mu^2} \psi \\ + (2\nu^2 - 4\Omega^2)\mu(1 - \mu^2) \frac{d}{d\mu} \psi + (4\mu^2 - 4 - 2\Omega^2 + \nu^2)\nu^2 \psi = 0. \quad (21)$$

This equation may be solved numerically for the eigenvalue Ω^2 as a function of ν , subject to the boundary conditions on ψ and its derivatives given in the following subsection.

c) Perturbed Boundary Conditions and Constraints on ψ

The perturbed boundary conditions used here are identical to those given in GLB for the case of no rotation. Following their derivation, we assume that the z coordinate of a surface of the layer varies sinusoidally (according to eq. [13]) around the mean value (a) with constant amplitude η_1 . Then one of the boundaries occurs at $z = a + \eta_1 \exp(i\omega t + ikx)$. The total pressure at this boundary, P , is always the external pressure, P_{ext} ; so $P_0(a) = P(a + \eta_1) = P_{\text{ext}}$. The equation of hydrostatic equilibrium now provides a constraint on ρ_1 and η_1 after integration over z from a to $a + \eta_1$:

$$\int_a^{a+\eta_1} \left(\rho_0 \frac{d}{dz} \psi_0 \right) dz \approx \int_a^{a+\eta_1} \frac{d}{dz} P dz$$

or

$$\eta_1 \left(\rho_0 \frac{d}{dz} \psi_0 \right)_{z=a} \approx P(a + \eta_1) - P(a) \quad (22)$$

for η_1 a small quantity. Here the dependence on $\exp(i\omega t + ikx)$ has been dropped from each side of the equation. Since $P(a) = P_0(a) + P_1(a) = P_{\text{ext}} + P_1(a)$, we have for a boundary condition

$$P_1(a) = -\eta_1 \left(\rho_0 \frac{d}{dz} \psi_0 \right)_{z=a}. \quad (23)$$

This may be combined with equations (3), (6), and the hydrostatic solution for $d\psi_0/dz$, which is

$$\frac{d\psi_0}{dz} = -4\pi G \rho_{00} H \tanh\left(\frac{z}{H}\right), \quad (24)$$

to give, after normalization and transformation to the independent variable μ ,

$$(1 - A^2)^2 \frac{d^2}{d\mu^2} \left(\frac{\psi}{\eta_1} \right) - 2A(1 - A^2) \frac{d}{d\mu} \left(\frac{\psi}{\eta_1} \right) - \nu^2 \left(\frac{\psi}{\eta_1} \right) + 4A(1 - A^2) = 0. \quad (25)$$

Here the derivatives are to be evaluated at $\mu = \pm A$. Recall that η_1 is simply a constant representing the magnitude of the perturbation around the hydrostatic solution. The variable ψ/η_1 will be independent of the magnitude of the perturbation for small perturbations ($\eta_1 \ll a$).

The equation of continuity gives a second boundary condition; namely,

$$i\omega\eta_1 = u_z(a). \quad (26)$$

This gives an equation for the third derivative of ψ at the boundary. It may be combined with equations (15) and (17), normalized and transformed to the independent variable μ , to give the equation

$$(1 - A^2)^3 \frac{d^3}{d\mu^3} \left(\frac{\psi}{\eta_1} \right) - 4A(1 - A^2)^2 \frac{d^2}{d\mu^2} \left(\frac{\psi}{\eta_1} \right) - (1 - A^2)\nu^2 \frac{d}{d\mu} \left(\frac{\psi}{\eta_1} \right) - 2A\nu^2 \left(\frac{\psi}{\eta_1} \right) + 4\Omega^2(1 - A^2) = 0 \quad (27)$$

for the derivatives of ψ at $\mu = \pm A$.

Finally, a third condition comes from the requirement that, at the boundaries, ψ must equal the external potential, which is a solution to Laplace's equation:

$$\psi_1(z > a) \propto \exp(-|kz|) \exp(i\omega t + ikx). \quad (28)$$

The potential at the boundary also satisfies Gauss's law in the approximation that the perturbed distribution of matter near the surface is confined to a thin plane; i.e.,

$$\frac{d}{dz} \psi_1(a+) - \frac{d}{dz} \psi_1(a-) = -4\pi G \rho_0 \eta_1. \quad (29)$$

Combining equations (28) and (29), we obtain (GLB)

$$|k\psi_1(a)| + \frac{d}{dz} \psi_1|_{z=a} = +4\pi G \rho_0 \eta_1. \quad (30)$$

The normalized, transformed boundary condition is thus

$$(1 - A^2) \frac{d}{d\mu} \left(\frac{\psi}{\eta_1} \right) + \nu \frac{\psi}{\eta_1} - 2(1 - A^2) = 0 \quad (31)$$

for the derivative evaluated at $\mu = A$.

Equations (25), (27), and (31) give the three derivatives of ψ/η_1 (normalized to the arbitrary but constant perturbation η_1) at each boundary in terms of the unknown values of ψ/η_1 at the boundaries. A solution for ψ/η_1 as a function of μ now follows from the three boundary conditions and from equation (21) (which may also be divided by the constant η_1), as long as $(\psi/\eta_1)(A)$, $(\psi/\eta_1)(-A)$, Ω^2 , and ν are specified. To determine the desired dispersion relation, i.e., Ω^2 as a function of ν alone, we must impose further conditions which involve our choice for the symmetry of the perturbation around the midplane.

The boundary conditions and equation (21) have symmetry properties about $\mu = 0$; i.e., symmetric perturbations have

$$\eta_1(-\mu) = -\eta_1(\mu); \quad \psi(-\mu) = \psi(\mu); \quad \frac{d}{d\mu}\psi(-\mu) = -\frac{d}{d\mu}\psi(\mu); \quad \text{etc.},$$

and antisymmetric perturbations have

$$\eta_1(-\mu) = \eta_1(\mu); \quad \psi(-\mu) = -\psi(\mu); \quad \frac{d}{d\mu}\psi(-\mu) = -\frac{d}{d\mu}\psi(\mu); \quad \text{etc.}$$

To determine the unstable modes, we seek symmetric perturbations by choosing Ω^2 and ψ/η_1 at a boundary to be such that

$$\left. \frac{d\psi}{d\mu} \right|_{\mu=0} \equiv \left. \frac{d^3\psi}{d\mu^3} \right|_{\mu=0} \equiv 0 \quad (32)$$

for various values of ν . Antisymmetric solutions where $\psi(0) = (d^2/d\mu^2)\psi(0) = 0$ were also calculated. These solutions were found to be stable against gravitational collapse ($\Omega^2 > 0$ for all ν) as they were in Simon (1965*a*), and they will not be discussed further.

III. RESULTS

For a variety of different layers, each specified by the single parameter A , we have obtained values of the normalized growth rate Ω as a function of the normalized wavenumber ν . The numerical methods are discussed in Appendix A. We expect our solutions to be identical to those of Simon (1965*a*) in the limit of $A = 1$, and we expect

$$-\Omega^2 \approx \nu A \quad (33)$$

in the limit of $\nu \rightarrow 0$ and $A \rightarrow 0$ as shown in Appendix B. Solutions with different A were found to differ most in the value of ν for a given Ω . Comparison of the results for different A is made easier if we use the product νA , which varies much less for given Ω than does ν .

It is noteworthy that the normalized quantities, Ω and ν , may be the same for different astrophysical problems which have different values of (P, σ) if the parameter A is the same in each case. In terms of these two physical parameters, we have from equations (7) and (9)

$$A = \left(\frac{\frac{1}{2}\pi G\sigma^2}{P + \frac{1}{2}\pi G\sigma^2} \right)^{1/2} = \left(1 + \frac{P}{\frac{1}{2}\pi G\sigma^2} \right)^{-1/2}. \quad (34)$$

The value of A therefore depends only on the ratio P/σ^2 . The actual growth rate (in s^{-1}) is given by

$$\omega = (-4\pi G\rho_{00}\Omega^2)^{1/2}, \quad (35)$$

and the wavelength (in cm) is

$$\lambda = \frac{2\pi H}{\nu}. \quad (36)$$

These depend on ρ_{00} in addition to A , so both parameters P and σ (as well as c^2) must eventually be specified in order to convert our numerical results to physical quantities.

In what follows, we discuss only the negative values of Ω^2 , which are the modes that grow exponentially. In all cases studied, Ω^2 became positive for sufficiently large ν or for antisymmetric perturbations (see above); but these results are not presented here.

The derived values of $-\Omega^2$ versus ν for $A = 0.01, 0.1, 0.5$, and 0.8 are shown in Figure 1. The corresponding result for $A = 1$ from Simon (1965*a*) is also shown. (Note that his normalization factor for the growth rate differs from ours by a factor of $\sqrt{2}$.) Clearly $\Omega^2 \approx -\nu A$ for small νA as expected, and the curves for $A \neq 1$ appear similar in form to the limiting case $A = 1$.

The value of ν at the point of the maximum growth rate, denoted here by ν_{MGR} , and at the crossover point where Ω^2 turns positive, denoted by ν_c , is such that the products $A\nu_{\text{MGR}}$ or $A\nu_c$ increase only slightly with increasing A . This is evident from Figure 1 but is shown more explicitly in Figure 2, which is the result of numerous calculations with A equal to 0.01, 0.04, and all numbers from 0.1 to 0.8 in steps of 0.1. Similarly, the square of the maximum growth rate, $-\Omega_{\text{MGR}}^2$, is shown as a function of A by a dashed line in Figure 2. These three curves are nearly parabolic and may be represented to a relative accuracy of $\sim 2\%$ in the interval $A = (0.01, 1)$ by the formulae

$$A\nu_{\text{MGR}} \approx 0.294 - 0.0197A + 0.173A^2, \quad (37)$$

$$A\nu_c \approx 0.639 - 0.129A + 0.490A^2, \quad (38)$$

$$-\Omega_{\text{MGR}}^2 \approx +0.139 - 0.0220A + 0.103A^2. \quad (39)$$

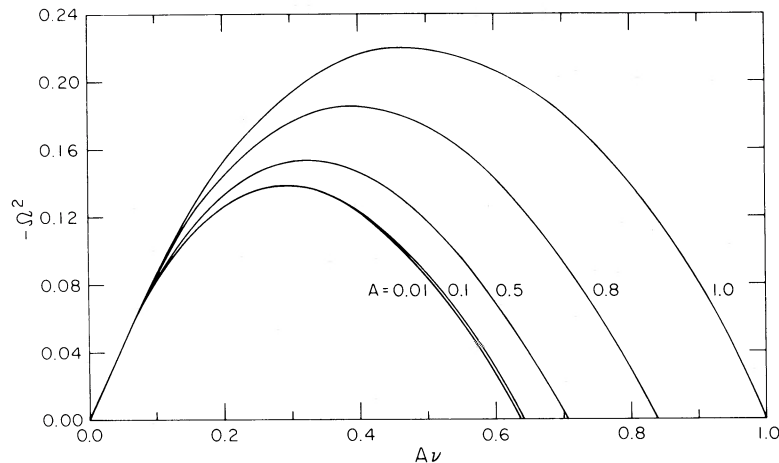


FIG. 1.—Squares of the normalized growth rates, $-\Omega^2$, are shown as functions of the product of A times the normalized wavenumber, ν . The parameter A depends on the sound velocity and column density in the layer, and on the external pressure. Large values of A characterize layers that are strongly self-gravitating.

We also find a nearly linear relationship between Ω_{MGR}^2 and $A\nu_{\text{MGR}}$, which is accurate to within 0.3% in the range $A = (0.01, 0.8)$ and is 5% too small at $A = 1$, i.e.,

$$-\Omega_{\text{MGR}}^2 \approx +0.468A\nu_{\text{MGR}} + 0.000476. \quad (40)$$

IV. VALIDITY OF APPLICATION TO ASTROPHYSICAL SHOCKS

We would like to know the conditions under which the linearized growth rates for the gravitational collapse of compressed gas behind an isothermal, plane-parallel shock will be the same as the growth rates derived in the preceding sections. The basic assumption is that, to first order in the perturbed quantities, the isothermal layer which accumulates behind a shock is similar to a plane-parallel layer with constant external pressure.

The plane-parallel nature of the calculation will be appropriate for most strong shocks that propagate into one side of a dense molecular cloud, since the layers behind these shocks are usually very thin. In some situations, however, surface instabilities may develop near the shock and the curvature of the layer may become significant (see Elmegreen and Elmegreen 1978). The propagation of a shock into a highly nonuniform cloud may also lead

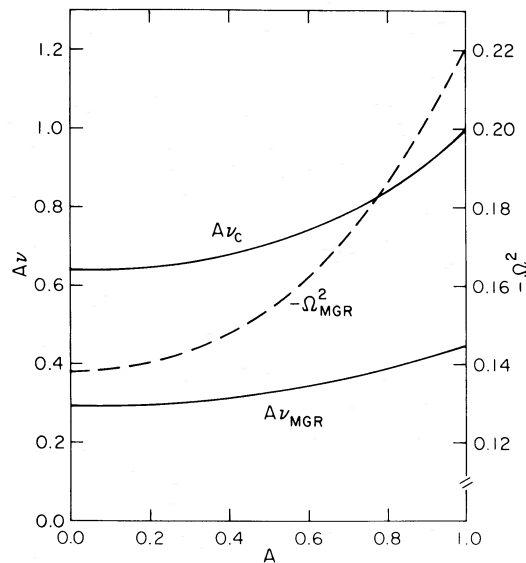


FIG. 2.—The square of the maximum normalized growth rate, $-\Omega_{\text{MGR}}^2$, is shown (*dashed line*) as a function of the layer parameter, A . The right-hand axis applies. Also plotted are the product of A and the normalized wavenumber at the point of maximum growth, ν_{MGR} , and A times the critical wavenumber, ν_c , i.e., where Ω^2 turns positive. The left-hand axis refers to these products $A\nu$.

to local curvature. Obviously, the present results do not apply to such cases. Nor should these results be applied directly to the gravitational collapse of swept-up material behind a moving spherical shock—even if the layer is much thinner than the radius of the sphere. The situation will not be the same as that considered here, because nearby points behind the shock will have a relative velocity directed parallel to the layer as a result of the sphere's expansion or contraction.

The validity of the assumptions concerning the equilibrium density distribution and the boundary conditions for the perturbation must also be considered. In the case of an accreting shock (where σ increases with time), the center of mass of the postshock layer will move relative to the postshock gas. This means that the equilibrium density distribution presented in § IIa must continuously adjust to the changes in σ . It can do this on the time scale for postshock sonic motions, $\sigma(\rho_{00}c)^{-1}$. This should be compared with the minimum time scale for the gravitational instability to occur, $(-4\pi G\rho_{00}\Omega_{\max}^2)^{-1/2}$. The application of our results to postshock layers requires that the equilibrium density distribution in the absence of perturbations be maintained on a time scale that is smaller than the gravitational growth time. This is equivalent to the requirement that $\sigma < \{2P[\pi G(8\Omega_{\text{MGR}}^2 - 1)]^{-1}\}^{1/2} \leq 1.4(P/\pi G)^{1/2}$ or that $A \leq 0.7$.

We also know that the boundary of the layer behind a steadily accreting shock will move away from the center of mass at some small velocity ϵ , which is of order $c(\rho_{\text{PS}}/\rho_{00})^{1/2}$ for postshock density ρ_{00} and preshock density ρ_{PS} . This means that the boundary of the layer really occurs at $z = a + \eta_1 \exp(i\omega t + ikx) + \epsilon t$ in the notation of § IIc. Equation (26) then should trivially include the velocity ϵ on each side, which does not change the relationship between η_1 and the perturbed boundary velocity $u_z(a)$.

The assumption that the pressure at each boundary is constant during the perturbation is valid to first order in η_1 . In the case of a layer behind a strong moving shock, the external pressure on the leading side will be dominated by the normal component of the ram pressure of the preshock gas. While this component varies sinusoidally with position x , the amplitude of the variation is second order in η_1 . Thus the pressure at the leading side is effectively constant. The pressure at the trailing side of the layer might be dominated by the thermal pressure in a relatively hot medium (e.g., an H II region or a supernova remnant). Since the sound velocity in this medium will be high, the trailing pressure will be able to adjust rapidly during the growth of the perturbation and it will also remain relatively constant at the layer's boundary. For a strong shock moving with a constant velocity, the total pressure on each side of the layer will be the same. Since we have assumed this to be the case here, the results apply only to shocks moving with constant velocity.

We also require that, for an evolving and collapsing layer, the masses of the perturbed elements must be much less than the total mass swept up by the shock. This ensures that the background force acting on any collapsing fragment will be the same as the force due to a uniform layer, as calculated. To check this, we must use a result from the following section. The maximum mass of a fragment that can collapse significantly in a time τ is given in equation (58) for $A\nu \leq 0.1$. This must be compared with the total mass in the layer, which is σ times the area of the shock, S . The result is that the maximum fragment mass will be less than the total mass in the layer, if $(\sigma/0.32 \text{ g cm}^{-2})(\tau/10^5 \text{ years})^2 < (S/1 \text{ pc}^2)^{1/2}$. This condition will be satisfied for a long time during the early stages in the growth of the layer. With a preshock density of 10^3 cm^{-3} and a shock velocity of 5 km s^{-1} , we require that $\tau < 3.7 \times 10^5 (S/1 \text{ pc}^2)^{1/6}$ years. After this time, the perturbations will no longer occur in a uniform background potential. The largest fragments will begin to coalesce by two-body interactions, and most of the material swept up by the shock will have become concentrated into several large clumps.

Perhaps the most obvious prerequisite for the validity of our results is that the formation and turn-on of massive stars in the layer must not have led to its disruption. Unfortunately, the point at which *massive* stars form cannot be determined simply from the parameters which specify the postshock layer. In view of the above constraints on τ and σ , it is possible that, in some layers, the formation of massive stars will occur after the present linearized calculation loses its validity.

V. ASTROPHYSICAL IMPLICATIONS

We consider the possibility that stars or clusters of stars may form as a result of compression and gravitational collapse in strong isothermal shocks. This process may be important at the interfaces between neutral clouds and expanding H II regions, supernova remnants, windswept bubbles, etc.; between two colliding clouds; or in a single cloud that is suddenly exposed to the high postshock pressure of a supernova blast wave or a spiral density shock. Observational evidence for this phenomenon is rapidly becoming available, and an attempt to summarize the current literature was made in § I.

What we can learn from the present results is the manner in which such a self-gravitating postshock layer begins to collapse. Elements of size $\lambda \approx 2\pi H/\nu_{\text{MGR}}$ dominate the collapse because their growth rate is the largest, while gaseous regions as small as $\lambda \approx 2\pi H/\nu_c$ or as large as the effective radius of curvature of the shock (i.e., the case $\nu \approx 0$ or $\lambda \rightarrow \infty$) grow more slowly. After an unstable region has collapsed significantly, however, the linearized calculations given here become inadequate. Most likely, these regions will continue to contract until they form small, near-spherical entities. They will be slightly deformed from perfect spheres by the background potential of the layer (see Callebaut 1975). At this stage, the criterion for further collapse will probably be the

usual Lane-Emden criterion for the collapse of a pressure-bounded isothermal sphere; i.e., collapse will occur when the mass in a sphere exceeds the critical value (Spitzer 1968)

$$M_{\text{SPH}} = \frac{1.18c^4}{G^{3/2}P_{\text{ext}}^{1/2}} \quad (41)$$

for external pressure P_{ext} .

As shown below, it is entirely possible that a sufficiently small element of mass can be unstable in the plane-parallel case but stable as an isothermal sphere. In this case, collapse will stop (after some oscillations) when the initially unstable sheet becomes a stable sphere. The formation of Bok globules, rather than stars, may be the only immediate result of such a low mass instability. Of course, other instabilities related to molecular reactions, heating and cooling changes, etc., may occur at this stage. Whether low-mass fragments actually do collapse even though they are stable by the criterion for an isothermal gas sphere is beyond the scope of this paper.

The onset of rapid star formation presumably occurs when unstable elements in the plane are too massive to be supported as spheres. To determine criteria for the occurrence of this phase, we compare M_{SPH} to the mass of an unstable element in the plane. For this latter quantity, we take the mass in a cylinder with diameter $\lambda/2$:

$$M = \frac{\pi}{4} \left(\frac{\lambda}{2}\right)^2 \sigma. \quad (42)$$

In terms of A and ν this becomes

$$M = \frac{2^{1/2}\pi^{3/2}}{8} \frac{c^4}{G^{3/2}P^{1/2}} \frac{A(1-A^2)^{1/2}}{\nu^2}. \quad (43)$$

Thus

$$\frac{M}{M_{\text{SPH}}} = 0.83 \frac{A(1-A^2)^{1/2}}{\nu^2}. \quad (44)$$

The mass of the fastest growing cylindrical element, denoted here by M_{MGR} , may be obtained by using ν_{MGR} in equation (43) or (44). We find that $M_{\text{MGR}}/M_{\text{SPH}}$ varies roughly as $A^3(1-A^2)^{1/2}$ (since $\nu_{\text{MGR}} \propto A^{-1}$), which has a maximum value at some A in the interval (0, 1). More precisely, we find

$$\text{MAX} \left[\frac{A(1-A^2)^{1/2}}{\nu_{\text{MGR}}^2} \right] = 1.97 \quad (45)$$

from our calculations. Thus

$$\frac{M_{\text{MGR}}}{M_{\text{SPH}}} < 1.64. \quad (46)$$

Similarly, the mass of the smallest unstable mass, M_{MIN} , is found by using ν_c in equation (43) or (44). We then obtain

$$\text{MAX} \left[\frac{A(1-A^2)^{1/2}}{\nu_c^2} \right] = 0.44, \quad (47)$$

so that

$$\frac{M_{\text{MIN}}}{M_{\text{SPH}}} < 0.36. \quad (48)$$

These results suggest that a critically unstable element, i.e., the one with the smallest mass, may end up as a stable sphere, regardless of A (however, recall the precautionary note stated above). The dominant unstable mass, i.e., the one that grows most rapidly, may also collapse to a stable sphere unless A increases to a value where $M_{\text{MGR}}/M_{\text{SPH}} = 1$. We find that this occurs first when

$$A = 0.54 \quad (M_{\text{MGR}} = M_{\text{SPH}}), \quad (49)$$

or, from equation (35),

$$\sigma = 0.91(P/\pi G)^{1/2}. \quad (50)$$

Thus, when a layer has grown so large as a result of accumulation behind a shock that σ^2/P is large and A exceeds 0.54, the most rapidly growing perturbation will be unstable even after it becomes nearly spherical. This may mark the onset of rapid star formation in shock-compressed layers. Equation (50) seems to be a better criterion than that given in Elmegreen and Lada (1977).

Even if $A < 0.54$, sufficiently large unstable regions ($\nu \approx 0$) will be too massive to form stable spheres after they collapse. These instabilities grow very slowly, however (see Fig. 1), and they may not be significant at all if the shock is short-lived. An upper limit to the unstable mass may be obtained by requiring that the growth rate of this mass be faster than the rate of significant change for the shock. We denote this upper limit by M_{MAX} and determine it as a function of the time scale τ for the duration or age of the shock. The criterion then takes the form

$$\omega^2 \equiv -4\pi G \rho_{00} \Omega^2 > \frac{1}{\tau^2}. \quad (51)$$

Using ρ_{00} from equations (7) and (9), and setting

$$\Omega^2 = -\beta(A)\nu A, \quad (52)$$

we may write this criterion in the form

$$\frac{c^2}{\nu} < \tau^2 4\pi G P \left(\frac{\beta A}{1 - A^2} \right). \quad (53)$$

All elements with such large values of ν (i.e., small wavelengths) will grow in a time τ or less.

The mass of such a perturbation may be obtained from equation (43). Since this mass scales with c^4/ν^2 , we may substitute equation (53) directly into equation (43) to obtain

$$M < 2(2)^{1/2} \pi^{7/2} G^{1/2} P^{3/2} \tau^4 \beta^2 A^3 (1 - A^2)^{-3/2}. \quad (54)$$

The right-hand side of equation (54) is taken to be M_{MAX} . Since $P/(1 - A^2)$ equals $\rho_{00}c^2$ and A^3 equals $(1 - P/\rho_{00}c^2)^{3/2}$, we see that $P^{3/2}A^3(1 - A^2)^{-3/2}$ equals $(\rho_{00}c^2 - P)^{3/2} = (\frac{1}{2}\pi G \sigma^2)^{3/2}$. Thus simplified, we have

$$M_{\text{MAX}} = \pi^5 G^2 \tau^4 \beta^2 \sigma^3. \quad (55)$$

Only elements with mass less than M_{MAX} will grow in a time less than τ . On the other hand, these elements will be unstable after collapse to a sphere, only if their mass exceeds M_{SPH} . Thus, when τ is sufficiently large that $M_{\text{MAX}} > M_{\text{SPH}}$, then all masses M in the range

$$M_{\text{SPH}} < M < M_{\text{MAX}} \quad (56)$$

will be significantly advanced to the point of complete collapse in the time τ .

We note that, when $A\nu$ for use in equation (53) is small—as it would be for typical values of $\tau \gtrsim 10^5$ years, $P \approx 10^{-10}$ ergs cm^{-3} , $c \approx 5 \times 10^4$ cm s^{-1} , and $A \approx 1$ —then we may use $\beta \approx 1$ from equation (33). A better approximation from Figure 1 is

$$\beta \approx 0.8, \quad A\nu \lesssim 0.1. \quad (57)$$

In this limit, M_{MAX} depends only on the column density in the layer and on the duration of the shock. It does not depend on the sound velocity in the layer or on the external pressure! Numerically, we have

$$M_{\text{MAX}} = 1 M_{\odot} \left(\frac{\tau}{10^5 \text{ years}} \right)^4 \left(\frac{\sigma}{2.8 \times 10^{-2} \text{ g cm}^{-2}} \right)^3, \quad (58)$$

where $\sigma = 2.8 \times 10^{-2}$ g cm^{-2} if a shock accumulates material with a preshock H_2 density of 10^3 cm^{-3} over a distance of 2.3 pc.

Evidently, M_{MAX} increases rapidly with the age of the shock—as τ^4 for constant σ , or as τ^7 in the case of a propagating shock where σ would be expected to increase linearly with time. The result is a time-dependent hierarchy of clustering, where the maximum collapsing mass continuously increases because of the inclusion (or perhaps coalescence) of more and more small fragments. Any subcondensations may have already collapsed to form pre-main-sequence stars or small globules like Bok globules.

After stars begin to form in the postshock layer, the isothermal equation of state used for the present calculation becomes inadequate. Stars may significantly heat or disrupt the gas, and the nature of any subsequent gravitational collapse should be quite complex. For this reason, the application of equation (51) to old, postshock regions which have already undergone significant gravitational collapse and star formation is probably not justified. Furthermore, the concept of a time-dependent maximum mass requires the use of plane-parallel geometry, for which the collapse rate goes to zero for very large perturbation lengths. Deviations from this idealized situation will be increasingly severe as the layer ages and massive self-gravitating fragments begin to appear.

VI. THE INFLUENCE OF MAGNETIC FIELDS

Magnetic fields may influence the results of this work by increasing the rms velocity in the layer. However, if the effective equation of state in the layer is determined primarily by magnetic fields, i.e., $P = \rho v_A^2$ for a constant Alfvén velocity v_A , these results will not change significantly: The dimensionless growth rates and wavenumbers are independent of the constant value of P/ρ , as are the unstable masses relative to M_{SPH} . Thus the criteria given in equations (49) and (50) are independent of the source of the rms motion in the layer. Even M_{MAX} is independent of a constant P/ρ , although, in general, the mass from equation (43) does depend on this velocity.

Of course, it is important to consider whether pressure from a magnetic field could ultimately prevent star formation. If a large cloud is initially supported by a magnetic field, then highly compressed gas in the part of an isothermal shock that propagates along the field will be greatly enhanced in gravitational energy density compared with magnetic energy density (see Elmegreen and Lada 1977). The initial stages in the collapse can then occur without field restraint. Once the collapse begins, the postshock density will increase even more; as a result, the ionization fraction will decrease and the rate of field diffusion out of the layer will increase. The field can then leak out of the gas, and star formation can proceed. Shocks that propagate in a direction perpendicular to the field will result in less postshock compression than do those shocks which move along the field. Infinitesimal gravitational instabilities of the type discussed in this paper will not be changed at all for collapse along the field (which now lies in the plane of the layer). However, the lower postshock density in this configuration will lead to a longer magnetic diffusion time behind the shock, and the final configuration of a collapsing layer may include substantial magnetic support. It remains unclear whether stars can eventually form behind shocks that propagate in a direction perpendicular to the field. Observational consequences of this difference between the two shock-field configurations were discussed in detail by Elmegreen and Lada (1977). It was suggested that this difference may lead to the observed directionality or sequence for star-forming events in large molecular clouds.

VII. CONCLUSIONS

The growth rate for gravitational instabilities in compressed layers has been calculated as a function of the wavelength of the instability. In dimensionless units, the layers are completely specified by a single parameter A equal to $\tanh(z/H)$ for scale height H and half-thickness z of the layer. The actual growth rates and sizes depend on the column density and sonic velocity of the layer, and on the external pressure. Simple formulae were given for the maximum growth rate, for the wavelength at this maximum, and for the critically unstable wavelength, as functions of A .

Some implications of these results for astrophysical situations were discussed, especially in relation to the possibility of star formation behind isothermal shocks. The critically unstable mass was found to be stable, if it collapses to a pressure-bounded isothermal sphere, regardless of the value of A . The mass of the most rapidly growing element will also be stable as a sphere, unless A exceeds 0.54. This threshold may mark the onset of rapid gravitational collapse and star formation behind the shock.

A maximum mass was derived for a plane-parallel fragment which undergoes significant collapse during the time τ , a characteristic time scale for the duration of the shock. Smaller masses will collapse in a time less than τ . Larger masses will not have enough time to collapse. The resultant value of M_{MAX} was found to be independent of the sonic velocity in the shocked layer and of the pressure that drives the shock. However, it depends strongly on τ and on the column density in the layer σ . This suggests that persistent shocks (τ large) or those which propagate into large dense clouds (σ large) may lead to massive star clusters. Short-lived shocks (τ small) or those which sweep up little material (σ small) may result only in the formation of Bok globules or small star clusters.

To the extent that the results in § IV were independent of the rms velocity in the layer, magnetic fields will not significantly alter our conclusions. We reemphasized the possibility originally suggested by Elmegreen and Lada (1977) that a sequence of star-forming events could exist in a molecular cloud owing to alignment and diffusion properties of a magnetic field.

B. G. E. gratefully acknowledges support by the Society of Fellows at Harvard University. D. M. E. thanks Zonta International for graduate support through an Amelia Earhart Fellowship.

APPENDIX A

METHOD OF CALCULATION

Equation (21)—along with the boundary equations (25), (27), and (31), and the constraint given by equation (32)—constitute an eigenvalue problem with eigenvalue Ω^2 and eigenvector $\psi = (\psi, \psi', \psi'', \psi''')$, where primes denote derivatives with respect to μ . The solutions presented here were obtained by iteration on a computer using the following algorithm.

First, a value of ψ/η_1 at one boundary was initialized arbitrarily, as was Ω^2 , and the higher derivatives of ψ/η_1 were determined at this boundary from equations (25), (27), and (31). The solution for $\psi(\mu)/\eta_1$ was then obtained by integration from $\mu = A$ to $\mu = 0$ in equal intervals of μ . A predictor-corrector scheme was employed in which values of ψ_1 at one point μ_1 were used to obtain values of ψ_2 at another, nearby point $\mu_2 = \mu_1 + \Delta\mu$ by iterating until convergence over the equations

$$\psi_2 = \psi_1 + \psi_1' \Delta\mu + \psi_1'' \frac{\Delta\mu^2}{2} + \psi_1''' \frac{\Delta\mu^3}{6} + (4\psi_1'''' + \psi_2''''') \frac{\Delta\mu^4}{120},$$

$$\psi_2' = \psi_1' + \psi_1'' \Delta\mu + \psi_1''' \frac{\Delta\mu^2}{2} + (3\psi_1'''' + \psi_2''''') \frac{\Delta\mu^3}{24},$$

$$\psi_2'' = \psi_1'' + \psi_1''' \Delta\mu + (2\psi_1'''' + \psi_2''''') \frac{\Delta\mu^2}{6},$$

$$\psi_2''' = \psi_1''' + (\psi_1'''' + \psi_2''''') \frac{\Delta\mu}{2},$$

and

$$\psi_2'''' = \psi_2'''''(\psi_2, \psi_2', \psi_2'', \psi_2''') \quad (\text{A1})$$

from equation (21). With these equations, the fifth-order derivative of ψ , i.e., $(\psi_2'''' - \psi_1'''')/\Delta\mu$, is continuously replaced by its average value in each interval $\Delta\mu$. The number of steps in the entire interval from $\mu = 0$ to $\mu = A$ was chosen to be sufficiently high that doubling the number of steps did not change the results (i.e., the final value of Ω^2) by more than 0.01%. It can be shown that this number of steps must be larger than $(1 - A^2)^{-1}$ for the Taylor-series expansions in equations (A1) to be valid. Generally, $\Delta\mu$ was taken to equal $-A/400$, and values of A less than 0.8 were used.

After the integration of $\psi(\mu)$ from $\mu = A$ to $\mu = 0$ was completed, the resulting value of $\psi'(0)$ was compared with zero. A second integration, using an initial value of $\psi(A)$ equal to 0.95 times the previous value (but using the same Ω^2), similarly gave a second value of $\psi'(0)$. The degree to which the second value of $\psi'(0)$ was closer to, or more deviant from, zero than was the first value of $\psi'(0)$ gave a correction factor to the input value of $\psi(A)$. Thus corrected, new values of $\psi(A)$ and $0.95\psi(A)$ gave more pairs of $\psi'(0)$ and thus further corrections to $\psi(A)$, until $\psi'(0)$ became arbitrarily close to zero, as required by condition (32). Typically, $\psi'(0)/\psi'(-\Delta\mu)$ was driven to the limit of computer accuracy, $\sim 10^{-14}$. The second condition, $\psi''(0) = 0$, was enforced in the same way; but in this case the two values of $\psi''(0)$ that were obtained after integrations with Ω^2 and $0.95\Omega^2$ were used to correct Ω^2 . Consecutive corrections to Ω^2 thus drove ψ'' to zero, while the first condition, $\psi'(0) = 0$, was enforced continuously by correcting $\psi(A)$.

The solution set $[\psi(A)/\eta_1, \Omega^2]$ was obtained for various values in the parameter space (ν, A) . Typically, five iterations over Ω^2 , each containing five iterations over $\psi(A)$, were required to drive $\psi'(0)$ and $\psi''(0)$ to zero, when completely arbitrary initial conditions on $\psi(A)$ and Ω^2 were used. Three and five iterations, respectively, were required for initial values that were obtained from previous solutions with similar (ν, A) .

APPENDIX B

THE LIMITING GROWTH RATE FOR SMALL νA

We seek the limit of Ω^2 as $\nu \rightarrow 0$ and $A \rightarrow 0$. Let ψ be of the form

$$\psi = \sum_i a_i \mu^{2i} \quad (\text{B1})$$

for the symmetric perturbations considered here. Equation (27) then gives to order A

$$-4\Omega^2 = A(24a_2 - 8a_1 - 2a_1\nu^2 - 2a_0\nu^2). \quad (\text{B2})$$

Thus $\Omega \rightarrow 0$ as $A \rightarrow 0$ for finite ν . The equation of motion may be used to give a recursion relation for a_i . For our purposes, we need only the coefficient of the μ^0 term, which must be set equal to zero from equation (21). Thus

$$24a_2 - 8a_1 - 4a_1\nu^2 + a_0\nu^4 - 4a_0\nu^2 = 0. \quad (\text{B3})$$

We now need a_0 and a_1 to order unity for use in equation (B2). Substituting equation (B1) into equation (31) gives

$$a_0 = \frac{2}{\nu} + \text{order}(A) \dots, \quad (\text{B4})$$

while equation (25) gives

$$a_1 = \frac{\nu^2 a_0}{2} + \text{order}(A) \dots = \nu + \text{order}(A). \quad (\text{B5})$$

Then equation (B3) gives $24a_2 \approx 16\nu + 2\nu^3 + \text{higher-order terms}$. Equation (B2) finally reduces to

$$\Omega^2 \approx -A\nu \quad (\nu \rightarrow 0, A \rightarrow 0). \quad (\text{B6})$$

REFERENCES

- Blaauw, A. 1964, *Ann. Rev. Astr. Ap.*, **2**, 213.
 Callebaut, D. K. 1975, *Mém. Soc. Roy. Sci. Liège*, **8**, 467.
 Elmegreen, D. M., and Elmegreen, B. G. 1978, *Ap. J.*, **219**, 102.
 Elmegreen, B. G., and Lada, C. J. 1977, *Ap. J.*, **214**, 725.
 ———. 1978, *Ap. J.*, **219**, 467.
 Goldreich, P., and Lynden-Bell, D. 1965, *M.N.R.A.S.*, **130**, 7 (GLB).
 Habing, H. J., Israel, F. P., and de Jong, T. 1972, *Astr. Ap.*, **17**, 329.
 Herbst, W., and Assoua, G. E. 1977, *Ap. J.*, **217**, 473.
 Jensen, E. B., Strom, K. M., and Strom, S. E. 1976, *Ap. J.*, **209**, 748.
 Kutner, M. L., Tucker, K. D., Chin, G., and Thaddeus, P. 1977, *Ap. J.*, **215**, 521.
 Lada, C. J. 1976, *Ap. J. Suppl.*, **32**, 603.
 Lada, C. J., Dickinson, D. F., Gottlieb, C. A., and Wright, E. L. 1976, *Ap. J.*, **207**, 113.
 Ledoux, P. 1951, *Ann. d'Ap.*, **14**, 438.
 Loren, R. B. 1976, *Ap. J.*, **209**, 466.
 Mueller, M. W., and Arnett, W. D. 1976, *Ap. J.*, **210**, 670.
 Ögelman, H. B., and Maran, S. P. 1976, *Ap. J.*, **209**, 124.
 Roberts, W. W. 1969, *Ap. J.*, **158**, 123.
 Schwartz, R. D. 1977, *Ap. J. (Letters)*, **212**, L25.
 Simon, R. 1965a, *Ann. d'Ap.*, **28**, 40.
 ———. 1965b, *Ann. d'Ap.*, **28**, 625.
 Spitzer, L., Jr. 1942, *Ap. J.*, **95**, 329.
 ———. 1968, *Diffuse Matter in Space* (New York: Interscience).
 Woodward, P. R. 1976, *Ap. J.*, **207**, 484.

BRUCE G. ELMEGREEN and DEBRA MELOY ELMEGREEN: Center for Astrophysics, Harvard College Observatory and Smithsonian Astrophysical Observatory, 60 Garden Street, Cambridge, MA 02138